

CMS: hadronic calorimetry, jets, and \cancel{E}_T performance

V. Daniel Elvira¹ for the CMS Collaboration

Fermi National Accelerator Laboratory, P.O. Box 500, Batavia, IL 60555, USA
 e-mail: daniel@fnal.gov

Abstract. The CMS experiment [1] uses a general purpose detector designed for detecting the diverse signatures associated with Higgs production and new physics beyond the Standard Model. These processes are typically associated with final states containing a large missing transverse energy and several high energy jets. Here, we present a description and status report of the construction and testing of the CMS hadronic calorimeter system, as well as its ability to measure jets and \cancel{E}_T .

PACS: 29.40.Vj; 29.40.Mc; 29.40.Ka

1 Introduction

The CMS experiment [1] employs a general purpose detector with nearly complete solid angle coverage. The detector design is focused on a clean detection of diverse signatures from new physics by identifying and precisely measuring muons, electrons, photons, and jets over a large energy range and at high luminosity.

The physics program of CMS, and its discovery potential, is very broad. One of the main objectives is to find or rule out the Higgs Boson predicted by the Standard Model (SM) and the Minimal Supersymmetric Standard Model (MSSM). Figure 1 shows the statistical significance, S/\sqrt{B} (with S : signal and B : background), as a function of the SM Higgs mass for a 30 fb^{-1} sample and all decay channels. The $H \rightarrow b\bar{b}$ decay mode dominates in the low mass range $m_H \lesssim 150 \text{ GeV}/c^2$. But the Weak Boson Fusion (WBF) process has emerged as one of the most promising channels for finding the Higgs in the low to medium mass range, for its high significance and clear signal [2]. The production mechanism and decay:

$$pp \rightarrow jjH \quad (qq \rightarrow q'q'H), \quad H \rightarrow WW^*/ZZ^* \rightarrow l^+l^-\nu\bar{\nu}/l^+l^-l^+l^- \quad (1)$$

leaves a signature of four leptons (e, μ, \cancel{E}_T) with the distinct feature of a forward and a backward jet which tend to preserve the initial parton direction. Fig. 7 shows the η distribution of the forward jets: at least one of them is produced half of the time beyond $|\eta|=3$. The search for new phenomena and, in particular, the supersymmetric partners of quarks and gluons are also an important part of the CMS physics program. These processes typically produce events with large \cancel{E}_T and several high energy jets.

In this paper, we will describe the CMS hadronic calorimeter system and its ability to measure jets and \cancel{E}_T .

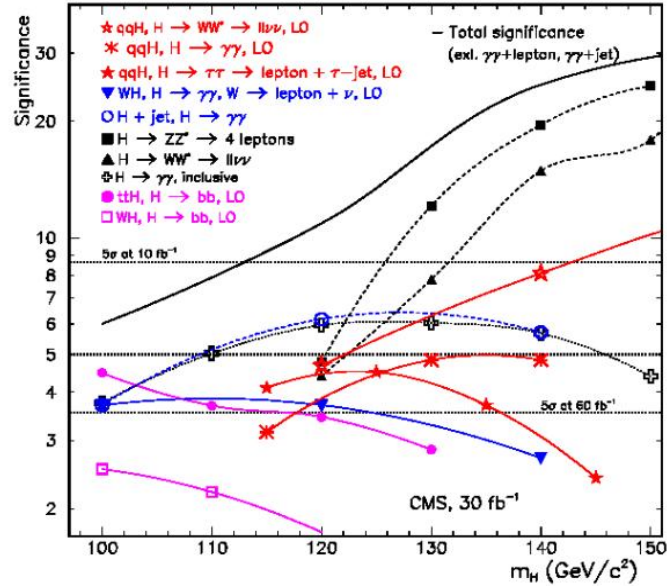


Fig. 1. Expected statistical significance as a function of the SM Higgs mass for a 30 fb^{-1} sample and all decay channels.

2 The CMS calorimeters

CMS has four kinds of hadronic calorimeters (HCAL) optimized for the detection of jets. The HCAL provides good segmentation and hermeticity, moderate energy resolution, and full angular coverage up to $\eta=5$ [1]. Figure 2 is a schematic of the full CMS detector. The Barrel Hadronic Calorimeter (HB) surrounds the electromagnetic calorimeter (ECAL), and covers the central pseudorapidity region up to $\eta=1.3$. The end regions are covered up to $\eta=3$ by the two End Cap Hadronic Calorimeters (HE). Pseudorapidity coverage is extended up to $\eta=5$ with the two forward calorimeters (HF), which surround the beam pipe 8.6 m from the interaction point. The HB and HE are located inside a 13 m long 4 T solenoid magnet, as shown in Fig. 2. Central shower containment is improved with an array of scintillators located outside the magnet which we refer to as the Outer Hadronic Calorimeter (HO).

2.1 The central barrel

The HB is divided into two cylindrical sections. These half-barrels consist of eighteen identical wedges made of flat absorber plates parallel to the beam axis. The body of the wedges is made of copper, but the innermost and outermost layers

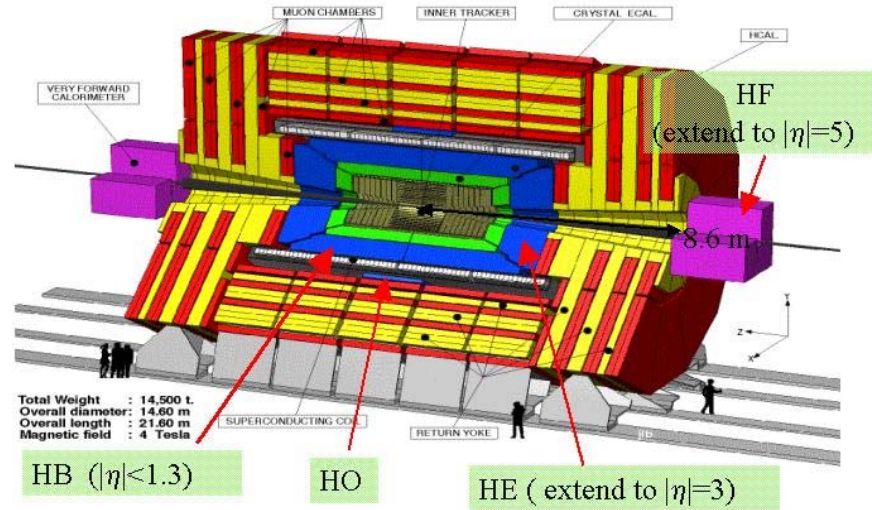


Fig. 2. Schematic of the full CMS detector.

are made of stainless steel for structural strength. The active readout scintillator tiles in each of the seventeen layers are divided into $\Delta\eta \times \Delta\phi = 0.087 \times 0.087$ segments. The HB has a pseudorapidity coverage of 1.3, a minimum depth of $5.8 \lambda_I$, and the energy resolution for single pions is approximately $120\%/\sqrt{E}$. Fig. 3 is a picture of one of the half-barrels, already built and assembled. A single wedge, also shown, is segmented into four 5° azimuthal and sixteen η towers.

2.2 The tail catcher

For the CMS detector, the total number of interaction lengths including the tracker, the ECAL and the HB is ~ 8 at $\eta=0$. Since approximately 5% of the energy of a 300 GeV pion would be leaked outside the HB, CMS has incorporated the HO or outer calorimeter to improve shower containment. It consists of two layers of scintillators in the central muon ring (Ring 0) on each side of the first muon layer with the same tower granularity as the HB. Only one HO layer, beyond the first iron layer, is available in Rings 1-5. The total depth of the calorimeter system is thus extended to $\sim 11.8 \lambda_I$, with an improvement in both linearity and energy resolution ($\sim 27\%$ for 300 GeV pions [3]). Figure 4 shows the HO configuration studied in the 2002 HCAL test beam experiment.

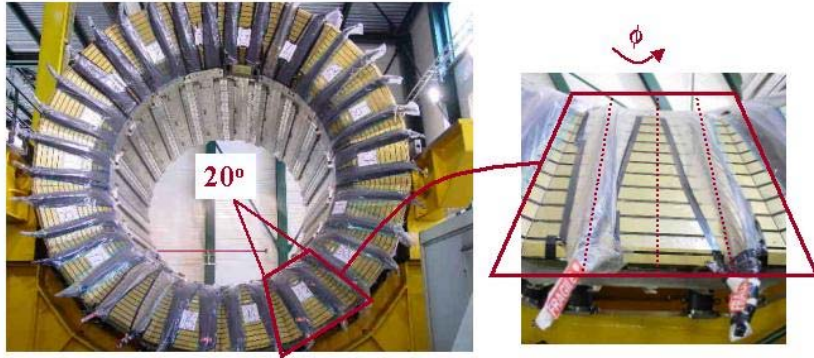


Fig. 3. A half-barrel hadronic calorimeter (HB). One wedge is segmented into four 5° azimuthal and sixteen η towers. It consists of seventeen layers of copper (steel for the first and last) and scintillator.

2.3 The end caps

The HE is a sampling calorimeter consisting of eighteen 20° modules, each made of nineteen layers of brass and scintillator. The HE extends the η coverage to 3, and has a minimum depth of $10 \lambda_I$. Its transverse segmentation is the same as for the HB and provides similar hadron energy resolution. The end caps are assembled and one of them installed on the end cap iron in surface hall, as shown in Fig. 5.

2.4 The forward calorimeters

The HF calorimeters are located 8.6 m from the interaction point. They are made of steel absorbers and embedded radiation hard quartz fibers, which provide a fast collection of Cherenkov radiation. The HF extends the η coverage to 5, where its depth is $\sim 9 \lambda_I$. It is divided into thirteen η towers and the azimuthal segmentation is 10° . The HF is under construction, with the fibre insertion expected to be finished by November 2003 (see Fig. 6).

The HF is a crucial tool for tagging forward jets to reduce QCD backgrounds in Higgs searches. Most of the interesting forward jets are very energetic for which the HF provides a reasonable energy resolution, i.e. 20% for 400 GeV pions.



Fig. 4. The Outer Hadronic Calorimeter configuration studied in the 2002 HCAL test beam experiment.



Fig. 5. The end caps are assembled and one of them installed on the end cap iron in surface hall.

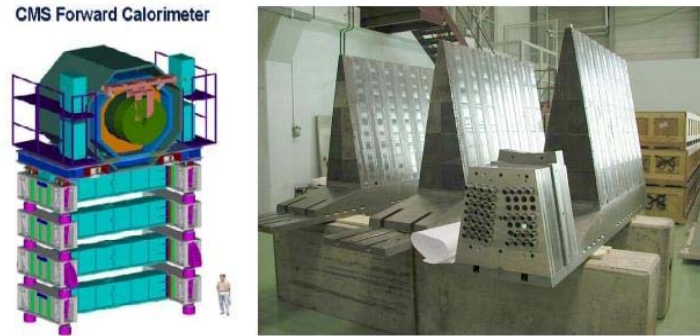


Fig. 6. Left: schematic of the forward hadronic calorimeter (HF). Right: HF modules in construction.

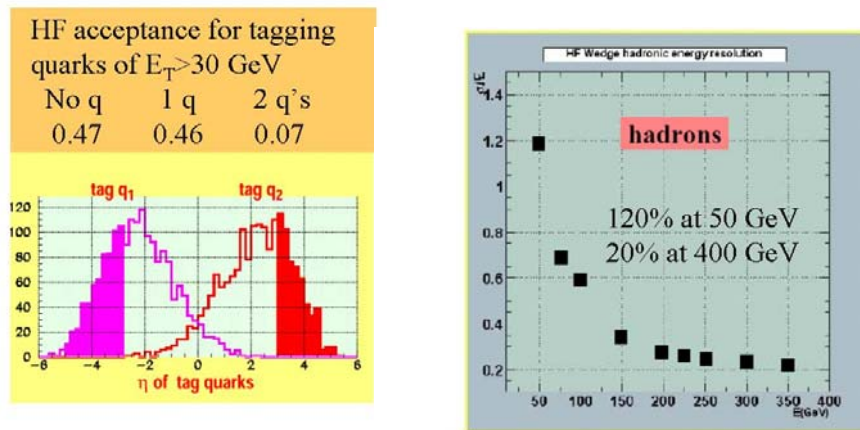


Fig. 7. Left: η distribution of the backward and forward jets associated with Higgs weak boson fusion decay. Right: fractional energy resolution for hadrons in the HF.

3 The 2002 HCAL test beam experiment

The 2002 HCAL test beam experiment was designed to study the performance of the CMS hadronic calorimeter. The detector was exposed to beams of π^- (20, 30, 50, 100, 300 GeV), electrons (20, 30, 50, 100 GeV), and muons (225 GeV) over a large energy range. More than 100 million events were read out with a 29.6 ns period, slightly longer than the 25 ns planned for CMS. A total of 144 HB channels (two wedges) and 16 HO channels were tested in a detector configuration which included an aluminum slab, representing the solenoid material, and a mock-up of the electromagnetic calorimeter (ECAL).

3.1 Detector Configuration

A picture of the experimental apparatus is shown in Figure 8. The beam direction is fixed in the laboratory frame, and a moving table used to change the relative direction of the beam with respect to the detector. This allows the beam to interact with different HB towers located at different ϕ and η . The beam line is equipped with two wire chambers and four scintillator tiles to trigger the events and monitor the beam position. The detector includes a mock-up of the ECAL, consisting of an aluminum box which contains a 7×7 PbWO_4 crystal matrix. The crystals are $23 \times 2.2 \times 2.2$ cm prototypes with a slightly smaller transverse section upstream than downstream. The box may be translated and rotated to allow the beam to be intercepted by any of the 49 crystals. The ECAL box is followed by two HB wedges positioned together as in the real CMS setup. An aluminum slab accounts for the solenoid material and precedes the outer hadronic calorimeter. The HO consists of two layers of scintillators surrounding an iron block which represents the first muon layer. The inner layer consists of only one panel (Ring 0 covering the central η region), and the outer layer of three panel (Rings 0, 1, 2 covering a larger η range).

For the HB and HO the light from the scintillators is transported to a Hybrid Photo Diode (HPD) through clear fibers. The signal is then processed by the Charge Integration Electronics (QIE) which gives a short output pulse.

3.2 Results and Performance

The lego plots in Fig. 9 show the energy, in ADC counts, deposited in the HB by a 100 GeV electron, a 300 GeV pion and a 225 GeV muon. Approximately 97% of the electron shower is contained in a 3×3 crystal matrix, while 99% of the pion shower is contained in a 5×5 tower array.

The distribution of pedestal widths is a measurement of the electronic noise in the HB. The mean of the noise is 0.875 ADC counts or 260 MeV, as illustrated in Fig. 10. Also shown is the pulse out of the QIE which is 90% contained in two 25 ns “CMS” time slices (time slices are 29.6 ns long in the test beam experiment).

An important measurement is the signal attenuation which is greater for central rapidity towers as the light travels longer distances from the scintillator tile to the QIE readout boxes. Fig. 11 shows an attenuation of approximately

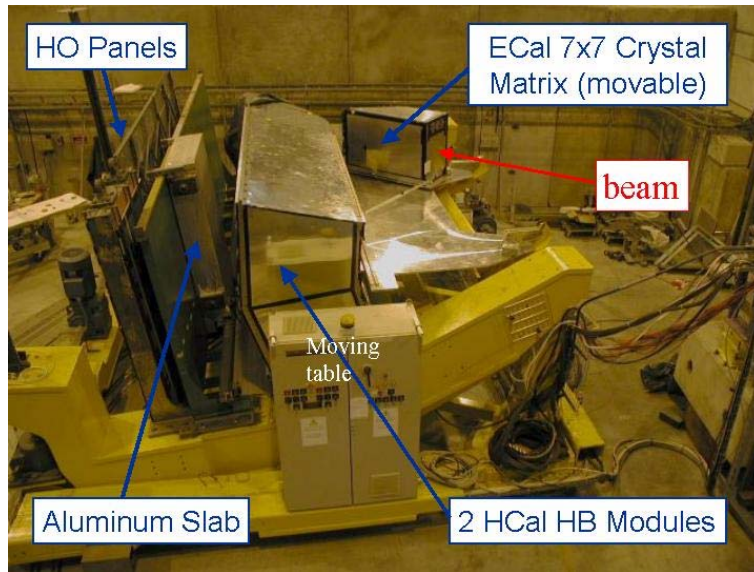


Fig. 8. Setup for the 2002 HCAL test beam experiment.

30% for the signal coming from the most central channel compared to the most forward.

The HO was studied with muons and pions. One of the goals was to determine if the muon measurement in the HO could be used as input information for the Resistive Plate Chamber (RPC) based muon trigger. The plot in Fig. 12 shows a pedestal subtracted muon peak against a pedestal (no beam) distribution. The potential for signal discrimination and background rejection of an RPC muon trigger using HO information is promising.

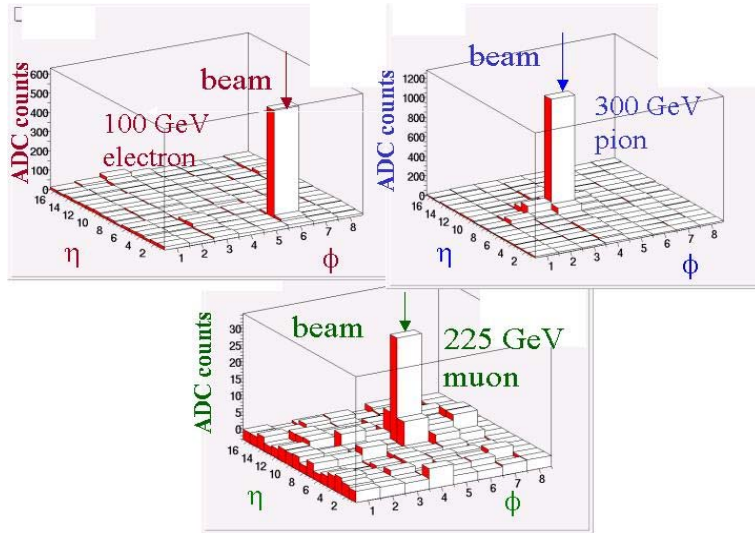


Fig. 9. Energy, in ADC counts, deposited in the HB by a 100 GeV electron, a 300 GeV pion and a 225 GeV muon.

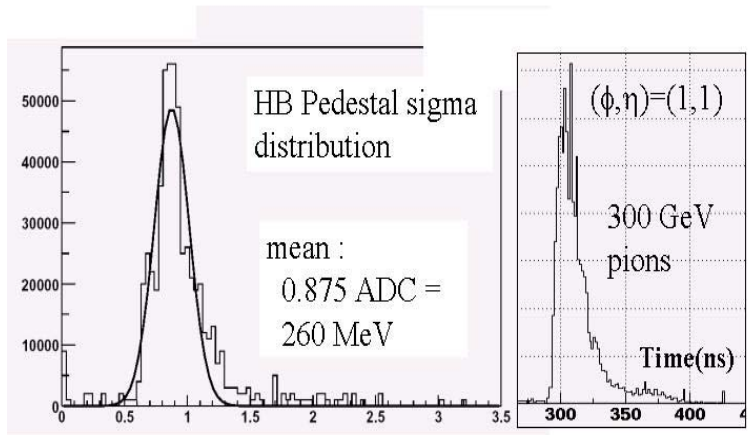


Fig. 10. Left: electronics noise distribution in a HB channel. Right: signal out of the Charge Integration Electronics (QIE).

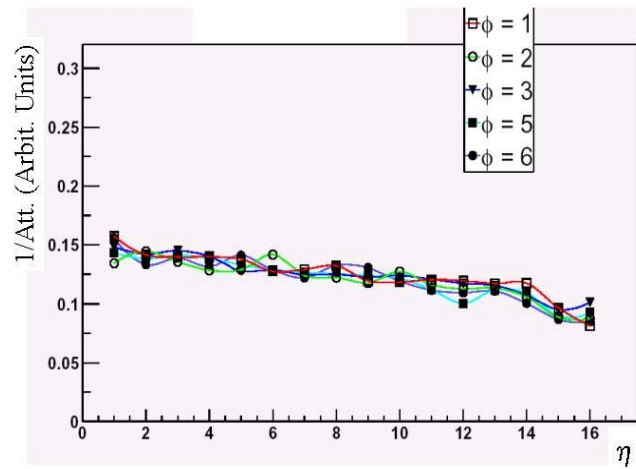


Fig. 11. The inverse of the response attenuation as a function of the read out channel in units of pseudorapidity.

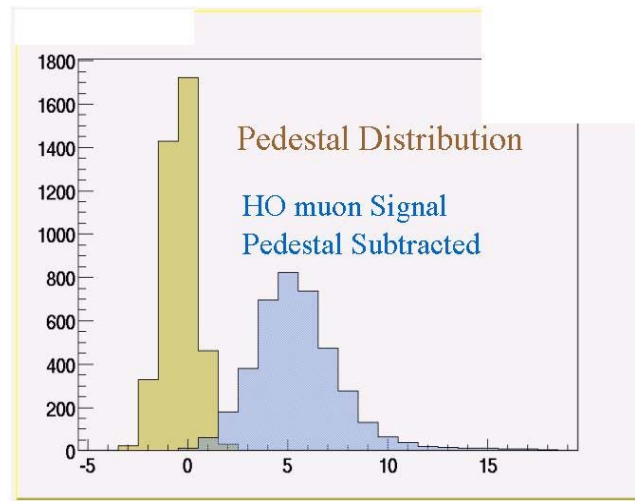


Fig. 12. HO pedestal subtracted muon peak against a pedestal (no beam) distribution.

3.3 Simulation and Data Comparisons

A crucial element for understanding the hadronic calorimeters is the development of an accurate Monte Carlo (MC) simulation. Simulations are critical to help in detector design and calibration, understanding resolution and linearity, as well as in data analysis. An additional goal of the GEANT4-OSCAR140 [4, 5] simulation of the 2002 HCAL test beam experiment is the validation of the GEANT4 physics by means of a comparison between the data and the Monte Carlo. The simulation includes all elements of the detector setup such as the beam line, the ECAL box, the HB wedges, the magnet mock-up, and the HO. The MC study mimics the data analysis and is based on a sample of 1 to 5 thousand π^- directed to the ECAL central crystal and the $(\eta, \phi) = (7, 3)$ HB tower (see Fig. 13). There is a caveat since the data actually corresponds to tower (9,4), for which longitudinal containment may be slightly larger. For illustration purposes, Fig. 14 displays a 10 GeV electron showering on the crystals and a 100 GeV pion showering on the HB.

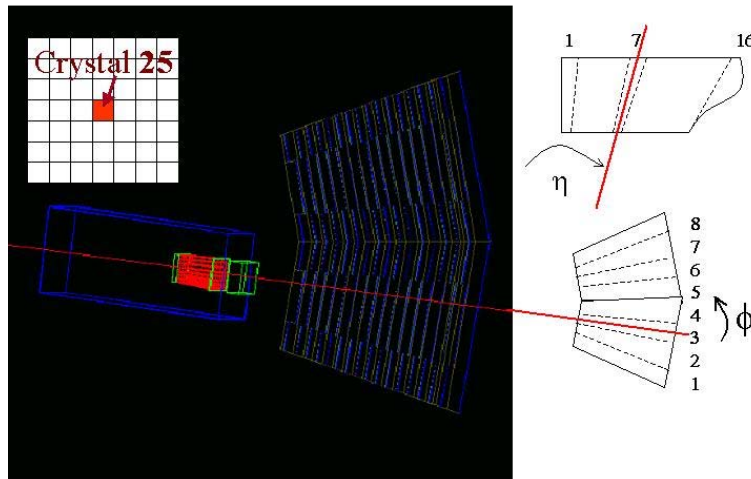


Fig. 13. Display of a particle traversing the central crystal of the ECAL box and the $(\eta, \phi) = (7, 3)$ tower of the test beam HB configuration, as simulated with GEANT4-OSCAR140.

Two of the most useful physics quantities to characterize a hadronic calorimeter are the hadron energy resolution and the linearity of the response as a function of energy. The pion energy was calibrated using a two steps procedure. The overall conversion factors from light in the scintillator to ADC counts was provided by a wire source (Co^{60}) passed next to each individual tile. Then, a residual correction was derived from a pion beam onto the (9,4) tower. Only those pions which deposited less than 2 GeV in the ECAL were selected. The same calibration factor was used throughout the HB. The ECAL calibration was performed similarly with a beam of 100 GeV electrons. Figure 15 shows the the

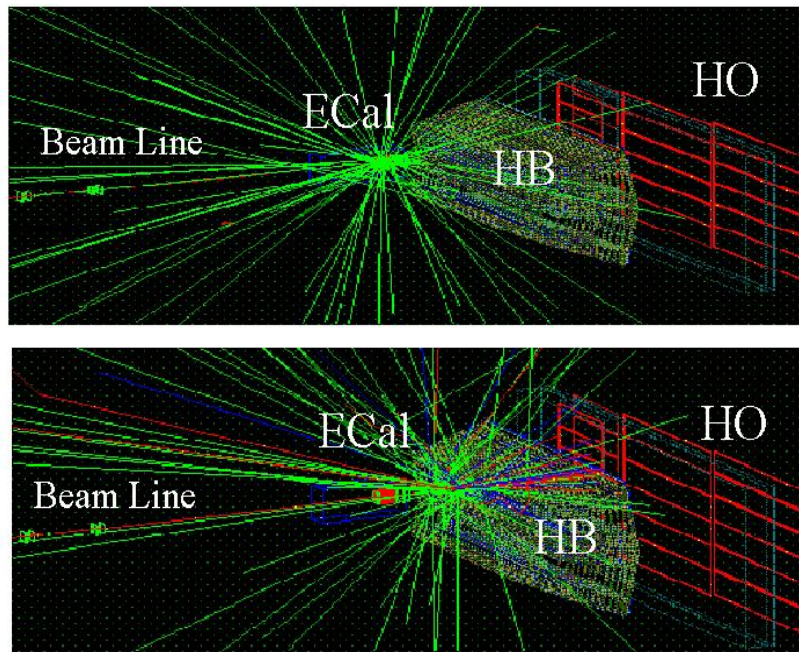


Fig. 14. Top: visualization of a GEANT4 electron shower (10 GeV) in the crystals. Right: a pion shower (100 GeV) in the HB.

energy deposited by a 50 GeV pion beam in the HCAL versus the energy deposited in the ECAL. There is a large concentration of pions depositing about 50 GeV in the HB. Many shower early in the crystals, as marked by the arrow. The smaller concentration of events at low energies comes from the muon and electron backgrounds. The two distributions are also apparent in a total energy distribution (calibrated ECAL+HB). From the background subtracted pion energy distribution we extract the resolution measurement. The fractional energy resolution for 50 GeV pions is 20.3%.

Figure 16 shows the measured fractional energy resolution versus the incident energy for π^- (open circles), compared with the same quantity as predicted by the GEANT4-OSCAR140 simulation. Both the electronics noise and the energy calibration procedure was modeled in the simulation. The agreement between data and MC is very good over the full energy range. The linearity, or calorimeter response to pions as a function of incident energy, is also shown in Fig. 16. The MC was normalized to the data at 100 GeV, and shows a faster turn on than the data. This is due to the GEANT4 modeling of hadronic showers which are shorter than observed in the data.¹ The systematic studies toward the completion of the pion response and linearity measurements will provide a powerful handle to

¹For this study, we have used OSCAR140 with a GEANT4 list of physics processes released in October 2001. The issue of short hadronic showers is still under investigation. Preliminary results using revised physics lists are encouraging.

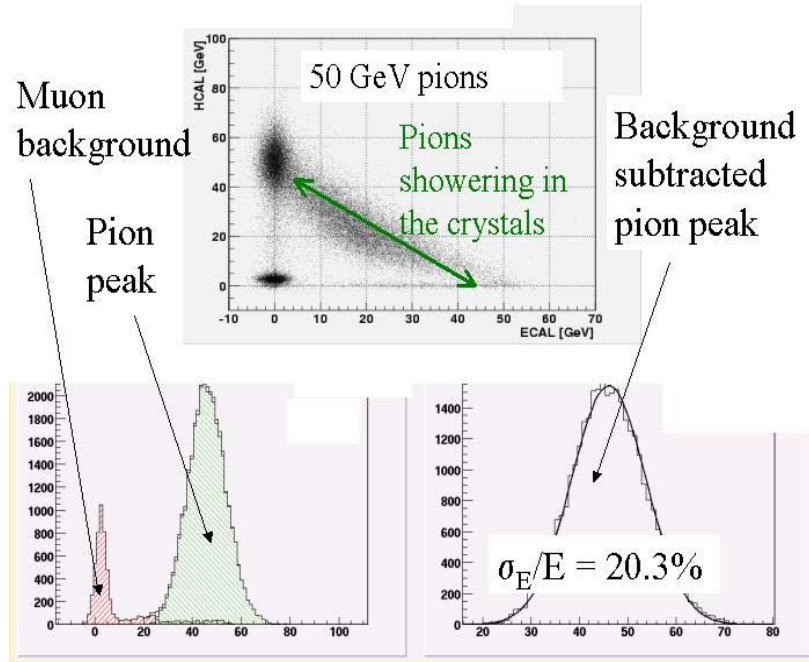


Fig. 15. Fractional energy resolution for 50 GeV pions measured from test beam data.

validate the GEANT4 physics models.

3.4 Summary of the test beam experiment

The goals for the 2002 HCAL test beam experiment have been met. We have operated at a clock rate of 33.79 MHz, slower than in the CMS experiment. We have done a source and beam calibration of the detector, tuned the weight of the first HB layer, studied the QIE pulse shape for pion showers, the response attenuation, and muon signals in the HO. The 2003 test beam experiment will improve the previous measurements, focus on the HB-HE boundary, and provide more control on the signal timing and backgrounds.

4 Physics Prospects: jets and \cancel{E}_T

The calorimeter performance to measure jets and \cancel{E}_T is of critical importance, as stated in previous sections. We generated single jets with PYTHIA 6.158 [6], simulated the detector effects with a low luminosity pile-up using CMSIM125-ORCA 620 [7, 8], and reconstructed jets using the $R=0.5$ fixed cone algorithm [9]. Figure 17 shows the energy dependence of the jet fractional energy resolution in the central η region, which is approximately 39% at 20 GeV and 12% at 100 GeV.

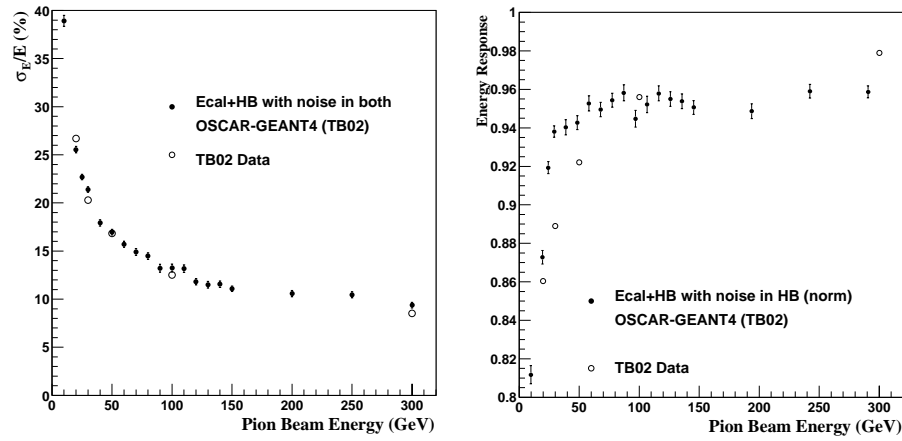


Fig. 16. Fractional energy resolution and response as a function of incident energy for π^- .

If the calibration of charged particles is improved by adding tracking information, the energy resolution also improves significantly. Missing transverse energy resolution, as a signature for neutrinos, was also studied using a SUSY sample with squark and gluino masses of ~ 500 GeV decaying to jets and \cancel{E}_T [10]. The current algorithm calculates \cancel{E}_T from the vector sum of all the calorimeter towers above 500 MeV. Type 2 \cancel{E}_T corrections, which use jet energy scale corrections for jets above 30 GeV as well as corrections for unclustered towers, are included in the analysis presented in Fig. 17. For low \cancel{E}_T events the resolution is about 20 GeV, increasing up to 40 GeV for events with \cancel{E}_T greater than 100 GeV.

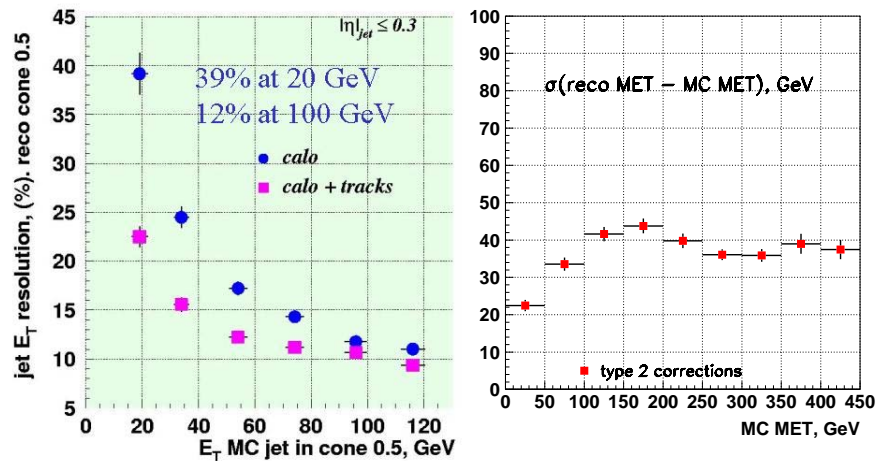


Fig. 17. Left: energy dependence of the fractional single jet energy resolution. Right: \cancel{E}_T resolution for SUSY events.

The two b-jet mass resolution was also studied using a MSSM sample where a higgs pair is produced from gluon fusion: $gg \rightarrow \phi \rightarrow hh \rightarrow 2\gamma + 2b$, with $m_\phi=300$ GeV and $m_h=125$ GeV [11]. CMSIM [7] and ORCA630 [8] were used for detector simulation including the pile-up associated with a luminosity of $2 \times 10^{33} \text{ cm}^{-2} \text{ sec}^{-1}$. Jets were reconstructed with a $R=0.5$ fixed cone algorithm, and only jets with $E_T > 30$ GeV were used. Figure 18 shows the b-jet fractional energy resolution, which is slightly worse than for the inclusive jet sample. Moderate improvement is achieved with the use of tracking information.

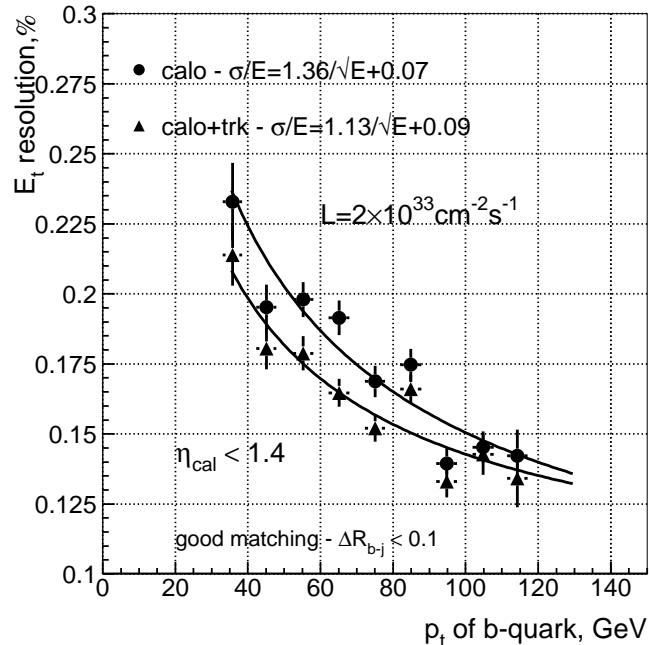


Fig. 18. Energy dependence of the b-jet fractional energy resolution.

Figure 19 shows the $b\bar{b}$ (h) mass resolution for jet reconstructed from calorimeter only information, 13.1%, and jets reconstructed from calorimeter and tracking data, 11%. These results for the $|\eta| < 1.2$ region correspond to a parton-to-calorimeter b-jet matching in (η, ϕ) space of $\Delta R < 0.1$. If the matching criteria is relaxed to $\Delta R < 0.3$, the resolution degrades to 14.7% and 13.3%, respectively.

5 Summary and plans

The HB and HE hadronic calorimeters have been completed and assembled. The HF fibre insertion is underway and will be finished by the end of 2003. The goals for the HCAL 2002 test beam experiment have been met, and the 2003 test beam program has started.

Another activity that is under way is the production of calibration, background, and physics samples toward the Data Challenge 2004 (DC04). The goal

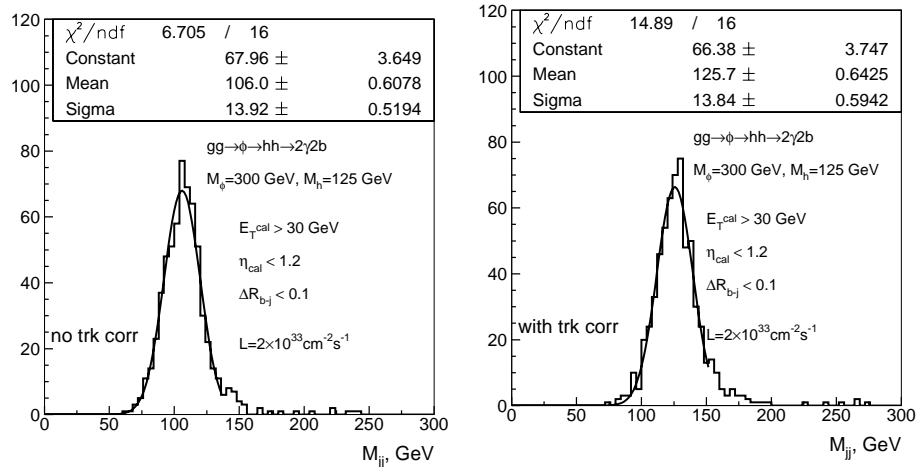


Fig. 19. Left: $b\bar{b}$ (h) mass resolution for jets reconstructed from calorimeter only information. Right: same for jets reconstructed from both calorimeter and tracking data.

of DC04 is to test the data reconstruction chain, validate the Monte Carlo, optimize detector parameters, develop particle algorithms and calibration techniques, as well as to perform physics prospect studies. Examples of HCAL oriented calibration and background samples are γ -jets, QCD dijets, $W + N$ jets, and top quark pairs as a source of high p_T W 's, jets and \cancel{E}_T . Physics samples to be generated correspond to prospect studies already in progress as well as others with good potential for detector or software optimization. For instance, $qqH \rightarrow WW^* \rightarrow l^+l^- \nu \bar{\nu}$, for optimization of the HF, development of forward jet tagging tools, and \cancel{E}_T studies. $W_L W_L$ scattering offers an alternative to the Higgs mechanism for symmetry breaking, with leptons, jets and \cancel{E}_T as decay products. The $Z' \rightarrow q\bar{q}$ process is very useful for energy resolution studies. SUSY samples, with squarks and gluinos, are a good source of energetic central jets and large \cancel{E}_T .

References

1. "The Compact Muon Solenoid Technical Proposal", The CMS Collaboration. CERN/LHCC 94-38, 1994.
2. "Study of low mass Higgs using $pp \rightarrow qqH$ at CMS", N. Akchurin *et al.*. CMS Note 2002/016
3. "Performance of Hadron Calorimeter with and without HO", Sudeshna Banerjee and Sunanda Banerjee. CMS Note 1999/063.
4. "GEANT4-A Simulation Toolkit", S. Agostinelli *et al.*, Nuclear Instruments and Methods A 506 (2003) 250-303.
5. Object oriented Simulation for CMS Analysis and Reconstruction. See <http://cmsdoc.cern.ch/cms/OSCAR/cmsgeant4.html>

6. See www.thep.lu.se/~torbjorn/Pythia.html
7. See cmsdoc.cern.ch/cmsim/cmsim.html
8. See cmsdoc.cern.ch/orca/orca.html
9. O. Kodolova and I. Vardanyan, private communication.
10. See cmsdoc.cern.ch/TDR/DAQ/daq.html
11. S. Nikitenko, private communication.